Arch. Metall. Mater. **70** (2025), 3, 1139-1142

DOI: https://doi.org/10.24425/amm.2025.154457

HEE YEON JEON[1], MYEONGJUN JI[1], YOUNG HWANGBO[1],
GUN-JAE LEE[2], YOUNG-IN LEE[1*]

SYNTHESIS OF BROOKITE TITANIUM DIOXIDE NANORODS USING SALT-ASSISTED ULTRASONIC SPRAY PYROLYSIS PROCESS AND THEIR PHOTOCATALYTIC ACTIVITIES

Here, We present the first-ever synthetic method based on the salt-assisted ultrasonic spray pyrolysis process of pure brookite TiO_2 nanorods. H_2TiF_6 and $NaNO_3$ were used as a titanium precursor and salt for the synthesis, the $NaNO_3$ contributes to the individual separation of primary nanostructures and the stabilization of brookite phase generated by the pyrolysis reaction of the precursor in a droplet. The synthesized nanorods were high crystalline and phase purity, as determined by X-ray diffraction and Raman spectroscopy studies. Scanning and transmission electron microscopy investigations showed the effect of the salt addition on the morphological features and the nanorods to have a one-dimensional morphology with an average diameter of about 10 nm. The photocatalytic activity of the synthesized brookite nanorod was tested employing the photodegradation of methylene blue under Xenon lamp irradiation. The results indicated that the brookite nanorod synthesized by salt-assisted ultrasonic spray pyrolysis was superior to commercial anatase nanoparticles.

Keywords: Titanium dioxide; Brookite; Nanorod; Ultrasonic spray pyrolysis; Photocatalysis

1. Introduction

Titanium dioxide (TiO_2), which is a widely used transition metal oxide semi-conductor, has attracted many applications such as photocatalysts, pigments, cosmetics, and dye-sensitized solar cells. It generally crystallizes in three natural crystalline polymorphs: anatase (tetragonal, I41/amd), rutile (tetragonal, P42/mnm) and brookite (orthorhombic, Pcab) [1,2]. Among the three polymorphs, brookite TiO_2 (B-TiO_2) has a higher degree of structural openness and the appropriate depth of electron trap [3,4]. This is an excellent advantage in separating and transferring the photoexcited electron-hole fairs. Thus, B-TiO_2 can be superior for photocatalytic degradation than anatase and rutile TiO_2.

In terms of the shape and size of the photocatalyst, one-dimensional (1D) TiO_2 nanostructures are of particular interest because of their high specific surface area and specifically size- and dimension-related properties. Hence, many works have focused on the synthesis and photocatalytic activities of 1D TiO_2 nanostructures [5,6]. Whereas the study related to 1D anatase and rutile TiO_2 is very active, there have been few studies on the properties and photocatalytic activities of 1D B-TiO_2 because it is the rarest phase with meta-stability and has difficulty in controllable synthesis, which requires complicated processes and specific condition.

The ultrasonic spray pyrolysis (USP) process has many advantages for synthesizing various oxide particles in large quantities and continuously, but is specialized in forming spherical particles of several microns in size due to the limitation of the size of fine droplets that can be sprayed [7,8]. Recent advancements have addressed limitations in the conventional USP method by introducing a salt-assisted ultrasonic spray pyrolysis (SA-USP) approach, where metal salts serve as a sacrificial template. This method has successfully produced various metal oxide nanoparticles approximately 10 nm in diameter [9-11]. However, there are few papers on synthesizing one-dimensional nanostructures using the SA-USP process.

In this study, we present a straightforward and efficient approach for synthesizing brookite-phase TiO_2 (B-TiO_2) nanorods via molten salt-assisted ultrasonic spray pyrolysis (MSA-USP). Using low-melting-point metal salts, such as $NaNO_3$ in the SA-USP process enabled crystallization under molten state

[1] SEOUL NATIONAL UNIVERSITY OF SCIENCE AND TECHNOLOGY, DEPT. OF MATERIALS SCIENCE AND ENGINEERING, SEOUL 01811, REPUBLIC OF KOREA
[2] DEPT. OF CARBON NEUTRALITY AND CORPORATE GROWTH SUPPORT, KOREA PLANNING & EVALUATION INSTITUTE OF INDUSTRIAL TECHNOLOGY, DAEGU 41069, REPUBLIC OF KOREA

* Corresponding author: youngin@seoultech.ac.kr

of the metal salt, facilitating atomic diffusion and promoting anisotropic crystal growth. The effect of the pyrolysis temperature on the size, shape, and crystal structure of the synthesized products was systematically investigated. In addition, their optical properties and photocatalytic activities were evaluated and compared to commercial anatase TiO_2 (A-TiO_2) nanoparticles.

2. Experimental

40 mM hexafluorotitanic acid solution (60 wt.% H_2TiF_6 in H_2O, Sigma-Aldrich) was used as the precursor solution for synthesizing B-TiO_2 nanorods and the sacrificial metal salt, sodium nitrate ($NaNO_3$, 99%, Sigma-Aldrich), was dissolved in the H_2TiF_6 solution at a concentration of 160 mM. The precursor solution was sprayed as fine droplets by an ultrasonic vibrator set to 1.7 MHz and then transported into the tube furnace with a quartz tube by O_2 gas. The internal temperature of the tube furnace was set in two stages. The first stage for drying the solvent was set at 200°C, and the second stage for thermal decomposition and crystallization was varied to 400, 500, 600, and 700°C to examine the effect of the temperature on the phase and morphology of final products. The prepared powder was collected using a filter paper inserted into the upper part of the tube and then washed more than 5 times with ultrapure water using an ultrasonicator (VC-505, Sonics & Materials, USA) and a centrifugal separator (1236R, Labogene, Korea) to remove the sacrificial metal salts.

The crystal structure of the synthesized product was characterized by X-ray diffractometer (XRD, X'Pert3 Powder, PANalytical, Netherlands) and Raman spectroscopy (LabRAM HR-800, HORIBA science, Japan). The size and morphology were characterized by field-emission scanning electron microscopy (FE-SEM; JSM-6700F, JEOL, Japan) and high-resolution transmission electron microscopy (HR-TEM, JEM-2100F, JEOL, Japan). The photocatalytic activities of the synthesized products were assessed by measuring the photocatalytic degradation rate of methylene blue (MB). The photodegradation test was performed using the solution prepared by mixing 50 mg of the synthesized powders with 100 mL of 2×10^{-5} M aqueous MB solution and a solar simulator equipped with a 300 W Xenon lamp and AM 1.5G Filter. After irradiation, a series of certain volumes of the mixtures were withdrawn and centrifugated. The UV/Vis spectrophotometer (UV-2600, Shimadzu, Japan) determined the residual concentration of MB in the centrifuged solutions.

3. Results and discussion

Fig. 1(a, b) presents the X-ray diffraction (XRD) patterns of powders synthesized by MSA-USP at different temperatures before and after the washing step. Before washing, $NaNO_3$ peaks were observed in the samples, whereas NaF peaks were detected at higher crystallization temperatures. The formation of NaF is anticipated as $NaNO_3$ decomposes at approximately 380°C, and fluorine is present in the precursor. In Fig. 1(b), the presence of the brookite phase is indicated by the brookite (211) peak at 32°. However, since the (210) peak of brookite overlaps with the (101) peak of the A-TiO_2 phase, Raman analysis was performed to confirm that the powders were pure brookite phase.

Fig. 1(c) shows the Raman spectra of the synthesized brookite and commercial A-TiO_2 nanoparticles (99%, 10 nm, MK nano) obtained using a 515 nm laser. Due to their distinct crystalline structures, the A-TiO_2 and B-TiO_2 phases exhibit unique peaks [12]. The A-TiO_2 exhibits a prominent peak at 142 cm^{-1}, corresponding to Ti-O-Ti bonds in bulk TiO_2. In contrast, the primary peak of the samples synthesized by MSA-USP appeared at 153 cm^{-1}, as a characteristic peak for brookite [13]. The decreased Raman peak intensity of the powder synthesized at 700°C can be explained by the alteration of surface bonding by the excessive formation of NaF during the MSA-USP process, which interferes with brookite crystallization [14].

FE-SEM was used to investigate the morphology of B-TiO_2 nanoparticles before and after washing treatment, as shown in Fig. 2. Before washing, the particles were micron-sized and spherical, which is a typical size and shape of powders synthesized by the spray pyrolysis process [15,16]. The powder was reduced to nanoscale by washing to remove sacrificial $NaNO_3$. This is because the sacrificial $NaNO_3$ was positioned between the primary particles during the spray pyrolysis, effectively suppressing particle agglomeration or sintering. The powder synthesized at 700 °C grew into a shell-like shape, indicating that the formation of NaF limited the particle growth inhibition by $NaNO_3$. HR-TEM analysis was performed to confirm the shape

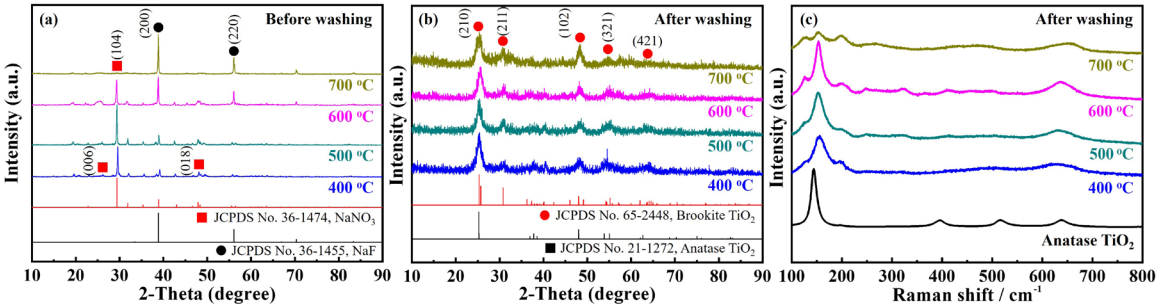

Fig. 1. (a, b) XRD patterns and (c) Raman spectra of the powders synthesized by MSA-USP at 400°C, 500°C, 600°C, and 700°C. XRD patterns contain results before and after washing treatment for removing sacrificial metal salts such as $NaNO_3$ and NaF. The Raman spectra results of the powders after washing are compared with a commercial anatase TiO_2 reference sample

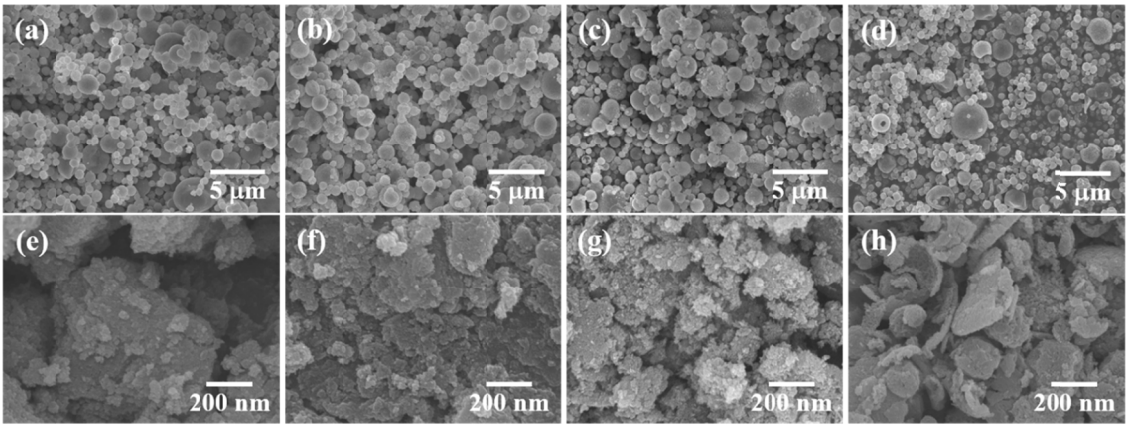

Fig. 2. FE-SEM images of the powders synthesized by MSA-USP at (a, e) 400°C, (b, f) 500°C, (c, g) 600°C, and (d, h) 700°C (a-d) before and (e-h) after removing the sacrificial metal salt

and crystal structure of the B-TiO_2 nanostructures synthesized at 600 degrees, and the results are shown in Fig. 3. As shown in Fig. 3(a), a low-magnification TEM image, the synthesized particles were confirmed to be rod-shaped with a diameter of about 10 nm and an aspect ratio of about 10 or more. Fig. 3(b) and 3(c) are HR-TEM images, and the synthesized nanorods showed a lattice spacing of 0.346 nm, consistent with the (111) crystal plane of B-TiO_2. The (111) and (211) crystal planes of B-TiO_2 can also be found from the results of the selected area electron diffraction (SAED) analysis as shown in Fig. 3(d).

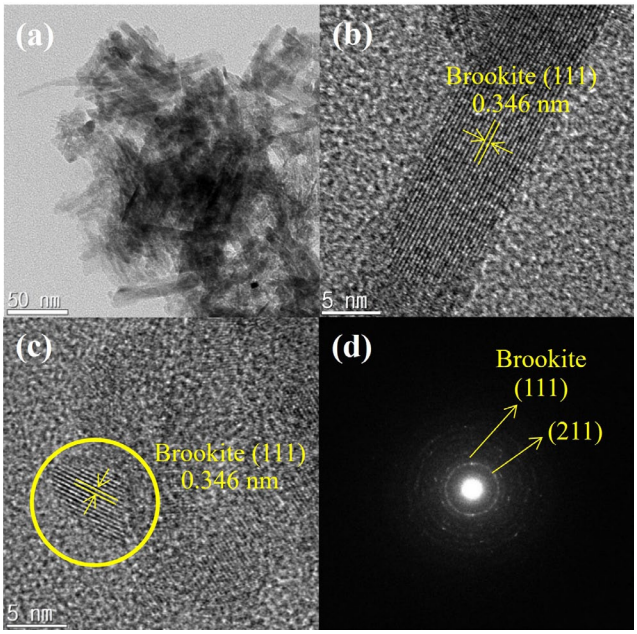

Fig. 3. (a) TEM image, (b, c) HR-TEM image, and (d) SAED pattern of the brookite TiO_2 powder synthesized by MSA-USP at 600°C after removing the sacrificial metal salt

The band gap of B-TiO_2 in its ideal state is approximately 3.2 eV, as predicted by Density Functional Theory [17]. However, experimentally measured values for B-TiO_2 generally range from 2.8 to 3.1 eV due to structural defects and oxygen vacancies, which influence its electronic properties [18,19]. Fig. 4(a, b) illustrates the UV-Vis absorbance and diffuse reflectance spectra of brookite TiO_2 powders synthesized by MSA-USP at various temperatures. The samples synthesized at 400°C and 500°C exhibit higher visible light absorption than those synthesized at 600°C. This may be due to the forming of an intermediate gap state induced by a higher defect density at a lower synthesis temperature. The band gaps of the synthesized powders, as determined by the Kubelka-Munk function, were measured to be 2.6, 2.85, and 2.9 eV for powders synthesized at 400°C, 500°C, and 600°C, respectively. As the synthesis temperature increased, the crystallinity of the powders also improved, leading to band gap values closer to those reported in previous literature.

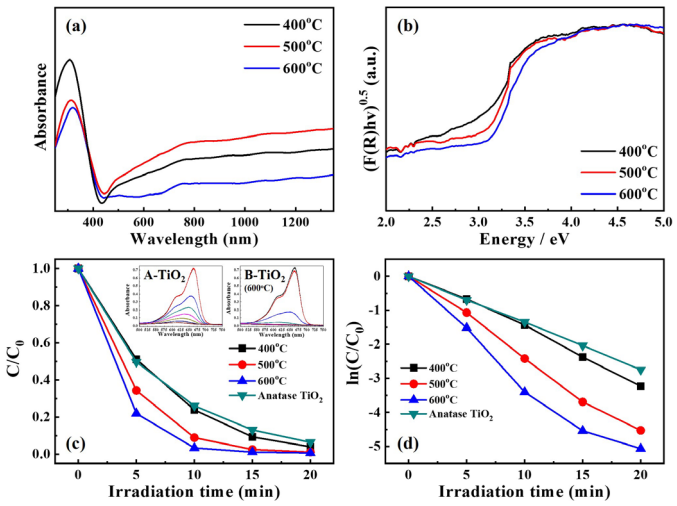

Fig. 4. (a) UV-Vis absorbance, (b) diffuse reflectance spectra, (c) photocatalytic activities, and (d) photodegradation rate constants (unit: k/min) of the brookite TiO_2 powders synthesized by MSA-USP at various temperatures after removing the sacrificial metal salt

Fig. 4(c) shows the photocatalytic properties of the B-TiO_2 nanorods synthesized at different temperatures, with commercial A-TiO_2 used as a reference. All synthesized samples exhibited photocatalytic performance either on par with or superior to the A-TiO_2, with the sample synthesized at 600°C showing the highest photocatalytic activity. The inset degradation graphs demonstrate that the 600°C-synthesized brookite TiO_2 degraded organic dyes in 10 minutes, while the reference required

30 minutes. The photodegradation rate constants (unit: k/min), derived from the slope of the degradation graph in Fig. 4(d), are 0.1617 ± 0.069 (400°C), 0.2462 ± 0.045 (500°C), 0.3402 ± 0.039 (600°C) and 0.1466 ± 0.036 (A-TiO_2). The B-TiO_2 synthesized at 600°C had a degradation rate approximately 2.3 times faster than the commercial A-TiO_2. These relatively excellent properties can be explained by the fact that brookite TiO_2 exhibits superior photocatalytic activity compared to anatase TiO_2 due to improved charge separation efficiency and high surface reactivity, as reported in previous studies [20,21]. In addition, higher synthesis temperatures promote enhanced photocatalytic performance, likely due to improved crystallinity and fewer defects in the material.

4. Conclusion

In this study, we successfully synthesized brookite TiO_2 (B-TiO_2) nanorods via molten salt-assisted ultrasonic spray pyrolysis (MSA-USP). We further investigated the effect of synthesis temperature on their structural, optical, and photocatalytic properties. The results demonstrated that B-TiO_2 nanorods could be synthesized at temperatures as low as 400°C, with the synthesis temperature significantly influencing the crystallinity, morphology, and electronic properties of the material. The band gap of B-TiO_2 was measured to be 2.6-2.9 eV, with the sample synthesized at 600°C showing the highest crystallinity and photocatalytic performance. The enhanced photocatalytic activity of B-TiO_2, particularly at 600°C, was attributed to the improved crystal structure and reduced defect density, making it an effective photocatalyst for organic dye degradation. These findings suggest that B-TiO_2 synthesized through MSA-USP can be a promising material for various photocatalytic applications, offering a viable alternative to traditional anatase TiO_2 in photocatalysis.

Acknowledgments

This research was supported by Seoul National University of Science and Technology.

REFERENCES

[1] T.L. Thompson, J.T. Yates, Chem. Rev. **106**, 4428-4453 (2006).
[2] X. Chen, A. Selloni, Chem. Rev. **114**, 9281-9282 (2014).
[3] M. Landmann, E. Rauls, W.G. Schmidt, J. Phys.-Condes. Matter. **24**, 195503 (2012)
[4] T. Zhu, S.P. Gao, J. Phys. Chem. C. **118**, 11385-11396 (2014).
[5] M. Ge, C. Cao, J. Huang, S. Li, Z. Chen, K.Q. Zhang, S.S. Al-Deyab, Y. Lai, J. Mater. Chem. A. **4**, 6772-6801 (2016).
[6] Z. Yu, H. Liu, M. Zhu, Y. Li, W. Li, Small. **17**, 1903378 (2021)
[7] M. Ji, Y.H. Choa, Y.I. Lee, Ultrason. Sonochem. **74**, 105557 (2021).
[8] S.R. Ardekani, A.S.R. Aghdam, M. Nazari, A. Bayat, E. Yazdani, E. Saievar-Iranizad, J. Anal. Appl. Pyrolysis. **141**, 104631 (2019).
[9] C. Panatarani, I.W. Lenggoro, K. Okuyama, J. Nanopart. Res. **5**, 47-53 (2003).
[10] G.H. An, T.Y. Hwang, J. Kim, J.B. Kim, N. Kang, S. Kim, Y.M. Choi, Y.H. Choa, J. Alloy. Compd. **583**, 145-150 (2014).
[11] Y. Hwangbo, Y.I. Lee, J. Alloy. Compd. **771**, 821-826 (2019).
[12] M. Choi, J. Lim, M. Baek, W. Choi, W. Kim, K. Yong, ACS Appl. Mater. Interfaces **9**, 16252-16260 (2017).
[13] G.A. Tompsett, G.A. Bowmaker, R.P. Cooney, J.B. Metson, K.A. Rodgers, J.M. Seakins, J. Raman Spectrosc. **26**, 57-62 (1995).
[14] H. Yang, F. Chen, Y. Jiao, J. Zhang, Chem. Eng. J. **214**, 229-236 (2013).
[15] A.L. da Silva, F.J. Trindade, J.L. Dalmasso, B. Ramos, A.C.S.C. Teixeira, D. Gouvêa, Ceram. Int. **48**, 9739-9745 (2022).
[16] V.L. Kurichenko, E.V. Argunov, D.Y. Karpenkov, E.A. Kolesnikov, Adv. Powder Technol. **35**, 104461 (2024).
[17] M. Manzoli, F.S. Freyria, N. Blangetti, B. Bonelli, RSC Adv. **12**, 3322-3334 (2022).
[18] H. Tang, K. Prasad, R. Sanjinès, P. E. Schmid, F. Lévy, J. Appl. Phys. **75**, 2042-2047 (1994).
[19] Z.Y. Yang, Y. Tao, T. Chen, H.J. Yan, Z.X. Wang, Phys. Chem. Chem. Phys. **15**, 2105-2108 (2013).
[20] Z. Li, S. Cong, Y. Xu, ACS Catal. **4**, 3273-3280 (2014).
[21] J. Vequizo, H. Matsunaga, T. Ishiku, S. Kamimura, T. Ohno, A. Yamakata, ACS Catal. **7**, 2644-2654 (2017).